IPPI
Polyolefins Journal, Vol. 9, No. 2 (2022)
DOI: 10.22063/POJ.2022.3009.1201
ORIGINAL PAPER

Preparation and characterization of nano WO_3/Bi_2O_3/GO and $BaSO_4$/GO dispersed HDPE composites for X-ray shielding application

Tohid Abdolahzadeh, Jalil Morshedian*, Shervin Ahmadi

Department of Polymer Processing, Iran Polymer and Petrochemical Institute (IPPI), P.O. Box 14975/112, Tehran, Iran

Received: 17 October 2021, Accepted: 29 January 2022

ABSTRACT

Researchers have studied the possibility of various polymer composites for radiation shielding applications. Lightness and non-toxicity of these materials are their significant advantages compared to Pb base traditional and common shields. In this research, polyethylene (HDPE)-based composites for shielding against X-ray radiations were prepared by utilizing several weight fractions of the nano tungsten oxide, bismuth oxide, and barium sulfate, which were decorated on nanographene oxide (10, 15, 20, and 25 wt%). The linear and mass attenuation coefficient values of samples were investigated experimentally with an X-ray tube at radiology energy ranges and estimated theoretically by using MCNP code (Mont Carlo Nanoparticle program). Results illustrate that by increasing the nanoparticles content, the linear attenuation coefficient parameter and the absorbed dose values increased dramatically. The shielding efficiency of the prepared samples has been shown by measuring the HVL values. Furthermore, the effect of sample thicknesses on the attenuation properties of nanocomposites was studied in this research. The morphological properties of the samples were evaluated with SEM. The collected results showed that the particle size of the nanoparticles used has a uniform dispersion in the polymer matrix. The mechanical properties of nanocomposite samples were characterized by DMTA and tensile test. Nanocomposites containing 20% and 25% of tungsten oxide and bismuth oxide particles reached to 88% and 90% dose absorption, respectively. **Polyolefins J (2022) 9: 73-83**

Keywords: Shielding; polyethylene; nanocomposite; linear attenuation; tungsten.

INTRODUCTION

X-rays and gamma rays have various applications in medical fields, healthcare and aerospace industries. So, protecting living bodies from harmful radiations is essential in nuclear sciences and industries for shielding against these radiations. The use of shielding materials is one of the practical ways to protect against radiation [1]. Lead-based shields are common equipment for personal protection against X-ray radiation during medical treatments [2, 3]. The heaviness, toxicity, and environmental hazards of lead are the most important drawbacks of utilizing lead-based shielding materials [4].

Polymer nanocomposites, which include metal or metal oxide fillers, are gaining considerable attention to be used as an alternative to traditional and common shields due to their specific properties such as light weight. Among different classes of materials utilized

*Corresponding Author - E-mail: J.Morshedian@ippi.ac.ir

for shielding applications [5], polyethylene-based composites are efficient in absorbing high-energy waves [6, 7]. Furthermore, polyethylene is low cost, recyclable, and nontoxic [8].

Polyolefins such as polypropylene, polyethylene, etc., have high chemical stability, which emanates from C-C bonds in their structure. Adding nanofillers into these materials leads to the achievement of nanocomposites with better mechanical/chemical properties. In addition, adding heavy metal fillers with shielding function to polyolefins creates a new application in these composites and enables them to perform as a shielding material against X-ray and gamma radiations [5, 6]. Mahmoud et al. fabricated polyethylene composites with the addition of 10% and 50% of lead oxide fillers [9]. According to the authors, the HDPE/PbO nanocomposite has lower effect on the density of polymer matrix. Eren and coworkers employed linear low density-polyethylene (LLDPE) as a matrix and utilized different weight percentages of PbO and WO_3 to fabricate shielding materials in regard to the electromagnetic radiation [10]. Kaloshkin and coworkers reported that UHMWPE composites loaded with boron carbide (B_4C) and tungsten nanoparticle have an appropriate attenuation toward gamma rays. According to the authors, there was a direct relationship between the linear attenuation coefficient and weight fraction [11]. Laurenzi and coworkers investigated the attenuation properties of nanocomposites containing MDPE matrix and the effect of various additives on the shielding mechanism [12]. The authors observed that the utilized polyethylene reduced the power of radiations through simulated sources such as GCR (galactic cosmic radiation).

Afshar et al. investigated the radiation attenuation performance of high-density polyethylene (HDPE) composites loaded with W, MoS_2, and B_4C particles. They demonstrated that flexible HDPE/45% W plate composite has a significant shielding efficiency against X-ray and gamma ray when comparing to the lead plate [13].

Here, HDPE-based nanocomposites loaded with different weight fractions of tungsten oxide, bismuth oxide, and barium sulfate (10, 15, 20, and 25% wt.) decorated on graphene oxide were employed and their shielding performance against X-ray radiations were investigated and evaluated by different methods. In this study, graphene oxide (GO) was fabricated by the modified Hummers method, and then nano $WO_3/Bi_2O_3/BaSO_4$ particles were decorated on the surface of GO. The use of a multi-step method involving decorating nanoparticles on graphene oxide and then blending reinforced composites containing GO/$WO_3/Bi_2O_3/BaSO_4$ at different filler loadings improved the attenuation performance of the composites fabricated. It was realized that decorating the surface of GO with the mentioned particles leads to the homogenous distribution and dispersion of nanoparticles in the polymer matrix and as a result developing lightweight polymeric composites against X-ray at various energies. The use of HDPE as a polymer matrix was high due to its excellent characteristics, such as low cost, process ability, and high physical and mechanical characteristics. HDPE-based shields can be used in the range of radiology wavelengths and in medical applications.

EXPERIMENTAL

Materials

To synthesize graphene oxide (GO) and nanoparticles, H_2SO_4, $KMNO_4$, ethanol, H_3PO_4, H_2O_2, graphite, acetone, NH3, and HCL were supplied from Merck. Nanobarium sulfate with an average particle size of 30-40nm was supplied from Sigma Aldrich Co. (USA). Nanotungsten oxide particles with an average diameter size of 20-30 nm was provided from Nanosany Corporation, Lewiston, USA. Nanobismuth oxide metal powder with an average size of 30-40 nm was provided from Zibo Jiashitai Technology Co. (China). High density polyethylene grade 52518 was supplied from Jam Petrochemical Company (Bushehr, Iran).

Graphene oxide synthesis

For producing GO, Hummer's method was employed. In this case, 2L H_2SO_4 was poured in a round-bottom flask then stirred (300 rpm) with heating at about 50°C. Afterward, 50 g $KMNO_4$ was added to the H_2SO_4. Next, 10 g graphite was added to the suspension. Thereafter, 110 mL H_3PO_4 was added to the pervious suspension, and after that the suspension was stirred (500 rpm) for 72 h with simultaneous heating (50°C). Next, the

suspension was poured in a vacuum ice-bound flask. Thereafter, 10 mL H_2O_2 was poured into the suspension slowly and after that the vacuum flask was filled with deionized water. The suspension was fixed for 48 h until the fillers precipitated. Subsequently, the suspension was filtered and the remained fillers on the filter paper were washed with HCL in order to remove the metal ions and washed with deionized water to neutralize the pH of the suspension. Finally, the resulting materials were dried for 1 h at 80°C in a heating oven and placed in the humidity reduction chamber for 48 h [14,15].

Decorating tungsten and bismuth oxide on GO (T-B-G)

In order to decorate nanotungsten and bismuth oxide on the nanographene oxide surface,1 gr GO was added into 100 mL ethanol and rotated at 50°C for 10 min (Scheme 1). Then, the allocated ethanol/GO suspension, 5 gr tungsten oxide, and 5 gr bismuth oxide were added to 250 mL deionized H_2O and reacted for 0.5 h at 60°C. Afterward, 40 mL NH_3 and 10 mL HCl were poured in the round-bottom flask, relatively. The final suspension was stirred for two days at 8°C. Then, the fillers were collected through filtration and were washed with deionized H_2O. Eventually, the achieved fillers, which labeled as T-B-G, were dried at 100°C. This method was employed in order to achieve better dispersion of nanoparticles on the polymer matrix [16].

Decorating barium sulfate on GO (Ba-G)

In order to decorate nanobarium sulfate on the graphene oxide, 1 g GO was added into 100 mL ethanol and rotated at 50°C for 10 min. Then, the mentioned ethanol/GO suspension, and 10 g barium sulfate were introduced in 250 mL deionized H_2O and reacted for 0.5 h at 60°C. Next, 40 mL NH_3 and 10 mL HCL were poured in the round-bottom flask, relatively. The final suspension was stirred for two days at 80°C. Thus, the fillers were gathered through filtration and washed with deionized H_2O. Eventually the achieved fillers, which labeled as Ba-G, were dried at 100°C (Scheme 1). This method was employed in order to achieve better dispersion of nanoparticles on the polymer matrix [16].

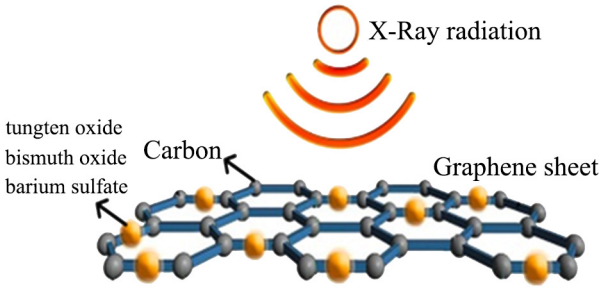

Scheme 1. Decorating nanoparticles on graphene surface and its efficiency against X-ray.

Preparation of nanocomposites samples

40 g of high density polyethylene with different weight fractions of synthesized graphene-decorated nanoparticles involving 0, 10, 15, 20, and 25% were mixed in an internal mixer at 200°C and 80 rpm for 10 min. As mentioned, the samples were prepared through melt blending method and then labeled according to Table 1. Samples were prepared in a sheet form with hot press. The dimensions of samples are 10cm×10cm with 1mm thickness. The thickness of the samples was controlled by laminating and overlay sheets at the desirable thicknesses.

Characterization

FTIR spectroscopy was performed using a Thermo Science, Nicolet Is5 infrared spectrophotometer (USA). The morphology of the synthesized samples was studied by a VEGA scanning electron microscope (SEM) (TESCAN, Czech Republic). The linear attenuation coefficient (μ) parameter of the prepared nanocomposites was measured by employing an X-ray tube (micro-CT imaging using their LOTUS-NDT scanner), and tensile properties were measured according to ASTM D638 (Instron, England) [17]. The linear attenuation value (μ) was achieved using equation 1:

Table1. Combination of the synthesized nanocomposite samples.

Sample	PE (wt. %)	T-B-G (wt. %)	Ba-G (wt. %)
PE-0	100	0	0
PE-A-10	90	10	0
PE-A-15	85	15	0
PE-A-20	80	20	0
PE-A-25	75	25	0
PE-B-10	90	0	10
PE-B-15	85	0	15
PE-B-20	80	0	20
PE-B-25	75	0	25

$$\mu = \frac{1}{x} \ln \frac{I_o}{I} \quad (1)$$

where x is the material thickness and I and I_0 are the deducted number of counts recorded in the detector with and without material between the detector and the source, respectively, and irradiation time was 60 s. By employing the linear attenuation coefficients, the mass attenuation coefficients (μ/ρ) will be achieved. The efficiency of X-ray shielding can be described by the half value layer (HVL) of a sample. The HVL is the thicknesses of an absorber that will reduce the radiation to half [18,19].

$$x_{1/2} = \frac{\ln 2}{\mu} \quad (2)$$

Furthermore, equivalent lead thickness for each sample was measured by employing the Beer-Lambert equation [14]:

$$(\mu / \rho)_{sample} \times \rho_{sample} \times X_{sample} = (\mu / \rho)_{Lead} \times \rho_{Lead} \times X_{Lead} \quad (3)$$

where $(\mu/\rho)_{Sample}$, ρ_{Sample}, x_{Sample}, $(\mu/\rho)_{Lead}$, ρ_{Lead} and x_{Lead} are the total attenuation of sample (with coherent scattering), the density of sample, the thickness of sample, the total attenuation of lead, the density of lead and the thickness of lead, respectively [16].

$$Hounsfield\ unit\ (HU) = 1000 \times \frac{\mu - \mu_{water}}{\mu_{water} - \mu_{air}} \quad (4)$$

where μ_{water} and μ_{air} are, respectively, the linear attenuation coefficients of water and air.

Therefore, a change of one Hounsfield unit (HU) displays a change of 0.1% of the attenuation coefficient of water since the attenuation coefficient of air is nearly zero.

This definition is for CT scanners that are calibrated with reference to water.

RESULTS AND DISCUSSION

FTIR study of GO, tungsten oxide, bismuth oxide, barium sulfate, T-B-G, Ba-G

To peruse the decoration of tungsten and bismuth oxides on the surface of graphene oxide, FTIR spectroscopy was employed. Recorded spectrums for GO, tungsten oxide, bismuth oxides, and T-B-G can be seen in Figure 1. According to the obtained spectrum of GO, the specific peak in 3200-3600 cm^{-1} is due to the hydroxyl segment of alcohols and phenols, and the bands at 1630 and 1725 cm^{-1} are related to the C=C and C=O bonds of aromatic rings and carboxylic groups, respectively. The peaks obtained at 1050 and 1200 cm^{-1} are due to the C-O bonds in epoxide and alcohols groups [15]. In the investigated spectra, the sharp peaks at 2800 and 2900 cm^{-1} correspond to the C-H stretching vibration [16]. These results demonstrate successful producing of GO. In addition, FTIR analysis of tungsten oxide and bismuth oxide can be seen in Figure 1. With comparing the FTIR spectra of GO, tungsten oxide, bismuth oxide and T-B-G, it can be seen that the intensity of the OH group of T-B-G is less than that of tungsten oxide, bismuth oxide, and GO. These results admit the reaction between GO and tungsten oxide, bismuth oxide through hydroxyl segments.

Furthermore, in Figure 2, FTIR spectra of GO, barium sulfate, and Ba-G show that the intensity of the mentioned peaks especially the OH peak in Ba-G is lower than that in GO and barium sulfate. So, this indicates the reaction between barium sulfate and the functional groups of GO [16].

Shielding characterization of synthesized nanocomposite samples

Study on experimental and theoretical attenuation properties of samples toward X-ray radiation

Hounsfield units (HUs) are utilized in computed

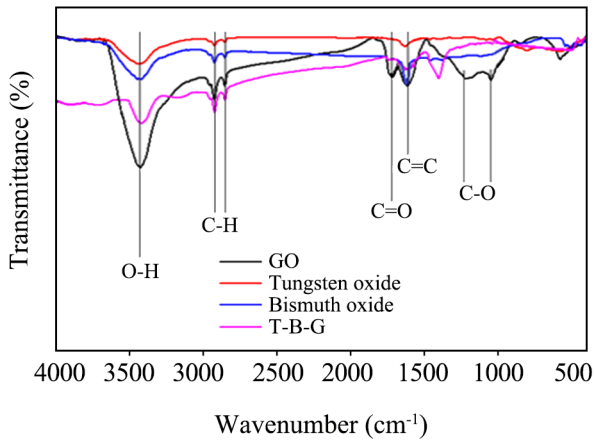

Figure 1. FTIR spectrums of graphene oxide, tungsten oxide, bismuth oxide, and T-B-G.

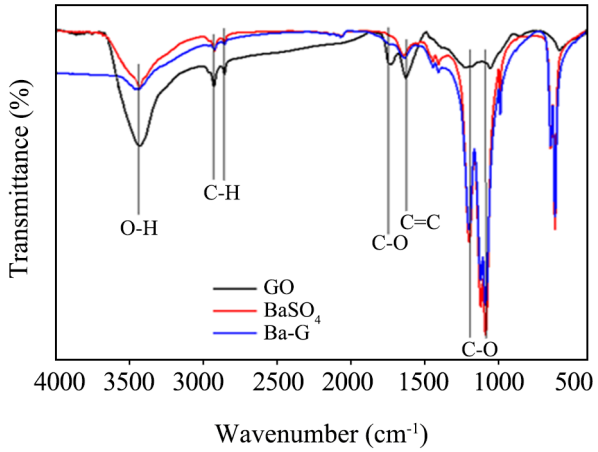

Figure 2. FTIR spectrums of graphene oxide, barium sulfate, and Ba-G.

tomography (CT) scanning to display CT numbers in a standard form and are quantitative scale for explaining radio density. They were obtained over the energy range of 60-120 kVp and are displayed in Table 3. PE-A-25 in 60 kVp demonstrated the highest Hounsfield unit (HU) value and expressed the most efficient shield among other samples. The measured and theoretical attenuation properties of the prepared nanocomposite samples are reported in Table 4. For this analysis, X-ray tube was used for radiology applications in the energy range of 50, 60, 80 and 120kvp. According to the obtained results, the linear attenuation coefficient values (μ) of the synthesized samples and their equivalent Pb values illustrated that 6 mm of PE-A-25 in the energy of 50 kV has the same attenuation behavior as 0.47 mm of pure Pb, which indicates that the operation conditions chosen to measure and calculate the linear attenuation coefficient were precise and suitable [18]. The Table 4 results illustrate that the linear attenuation coefficient values increased by increasing nanoparticles weight percentage. However, a smaller increase in μ value has been found by loading more nanoparticles content. Furthermore, tungsten/bismuth/GO-based nanocomposites showed higher μ values and better shielding efficiency in exposure of X-ray radiation

Table 2. Main FTIR peaks of GO, T-B-G and Ba-GO.

Wavenumber (cm^{-1})	Peak information
3200-3600	O-H stretching vibration
1630	C=C stretching vibration
1725	C=O stretching vibration
1050, 1200	C-O stretching vibration
2800, 2900	C-H stretching vibration

Table 3. Hounsfield Unit (HU) of fabricated nanocomposites.

Wavenumber (cm^{-1})	Peak information
3200-3600	O-H stretching vibration
1630	C=C stretching vibration
1725	C=O stretching vibration
1050, 1200	C-O stretching vibration
2800, 2900	C-H stretching vibration

compared to barium sulfate/GO nanocomposites.

The attenuation mechanism is directly related to the density of the nanocomposite, in which heavier atoms in the path of the photons lead to more interactions per unit length of the nanocomposite. According to the density results in Table 4, the density values of the fabricated samples increased by raising weight percentage of the high Z atomic numbers such as tungsten oxide, bismuth oxide, and barium sulfate nanoparticles. The mass attenuation coefficient values of the fabricated nanocomposite samples are gathered in Table 4. The results demonstrate that mass attenuation coefficient values move to higher values by raising the weight percentage of the utilized nanoparticles. The mentioned phenomena can be due to the increase in the nanoparticles weight percentage and the filler stability in the polymer media. These results confirmed that nanoparticles-filled samples performed better at all X-ray energies than the polymer matrix alone [18].

Efficiency of an X-ray shield can be explained in the terms of equivalent lead thickness [16]. So, in this section we evaluated the equivalent lead thickness values of the prepared nanocomposite samples in thickness of 6mm to camper their effectiveness against X-ray radiations. According to Table 4, increasing the filler weight fraction increases the equivalent lead thickness under similar energetic conditions (50, 60, 80, and 120 kVp). In the other hand, tungsten/bismuth-based nanocomposites showed higher equivalent lead thickness values [19,20]. In this case, the highest equivalent lead thickness is attributed to the sample PE-A-25 (Table). These results indicate the significant performance of the fabricated nanocomposites against X-ray radiation

To calculate theoretical μl (cm^{-1}) values, MNCPX code from Mont Carlo software was employed and discrepancy Δ% between the measured and simulated values of attenuation coefficient was calculated. According to the weight fraction of the elements and the density of the composites, the simulation was designed. The

Table 4. Attenuation experimental and theoretical results of the prepared nanocomposites*.

Sample	Energy(kVp)	Linear attenuation coefficient μ(cm^{-1})			Density (g/cm^3)	Mass attenuation μ/ρ (cm^{2}g^{-1})	Equivalent lead thickness(mm)
		Thickness(6mm)					
		Measured	MCNP	Δ%			
PE-0	50	0.073	0.072	0.93%	0.95	0.08	0.085
	60	0.062	0.061	0.75%		0.07	0.076
	80	0.050	0.049	0.74%		0.06	0.066
	120	0.041	0.040	0.82%		0.04	0.051
PE-A-10	50	0.243	0.240	1.23%	1.29	0.18	0.29
	60	0.224	0.221	1.31%		0.17	0.26
	80	0.172	0.170	1.19%		0.13	0.21
	120	0.135	0.133	1.11%		0.10	0.15
PE-A-15	50	0.352	0.347	1.4%	1.33	0.26	0.42
	60	0.316	0.313	0.9%		0.23	0.38
	80	0.255	0.252	0.8%		0.19	0.31
	120	0.184	0.181	1.6%		0.13	0.22
PE-A-20	50	0.366	0.362	0.95%	1.38	0.27	0.43
	60	0.328	0.324	1.24%		0.23	0.39
	80	0.267	0.263	1.33%		0.18	0.32
	120	0.194	0.191	1.13%		0.14	0.23
PE-A-25	50	0.383	0.376	1.72%	1.43	0.26	0.47
	60	0.351	0.345	1.55%		0.24	0.43
	80	0.297	0.292	1.47%		0.20	0.36
	120	0.225	0.221	1.67%		0.15	0.27
PE-B-10	50	0.163	0.161	1.17%	1.06	0.15	0.19
	60	0.144	0.141	1.41%		0.13	0.17
	80	0.128	0.125	1.79%		0.11	0.14
	120	0.091	0.089	1.56%		0.08	0.11
PE-B-15	50	0.205	0.202	1.35%	1.10	0.18	0.24
	60	0.188	0.185	1.19%		0.16	0.22
	80	0.162	0.160	1.39%		0.14	0.20
	120	0.131	0.129	1.61%		0.12	0.16
PE-B-20	50	0.215	0.212	1.32%	1.20	0.17	0.25
	60	0.196	0.194	0.94%		0.16	0.23
	80	0.162	0.160	1.15%		0.13	0.19
	120	0.128	0.126	0.99%		0.10	0.15
PE-B-25	50	0.261	0.257	1.47%	1.27	0.20	0.31
	60	0.234	0.230	1.29%		0.18	0.28
	80	0.206	0.l202	1.6%		0.15	0.24
	120	0.183	0.180	1.23%		0.14	0.18

model was assumed into multiple cubes as a matrix and orbs in the center of cubes as a particle. The 3D images simulated by the visual editor (VISED) MCNPX code are shown in Figure 3. This simulation was used to measure the photon flux stored in the detector with tally F4, F2. Tallying is the process of scoring the parameters of interest. For each answer the fractional standard deviation (fsd), relative error, is provided. Each tally is defined by an Fna number, where "n" is a unique number and "a" is the particle type. In the case of tally F4, this estimator uses the fundamental definition of influence as the number of particle-track lengths per unit volume. According to received data from tally F2 and employing equation 1, inlet surface flux and outlet surface flux of the materials in radiologic range energies were calculated and the linear and mass attenuation coefficient values were obtained. The achieved results demonstrated that there was a suitable adoption with negligible error between theoretical and experimental data. In other words, this comparison is the reason that shows that a suitable approach has been chosen for this research [16, 17, 18].

By applying linear attenuation coefficients, the HVL values were obtained. The results for HVL values are shown in Figure 4. According to the Table 4 results, the linear attenuation coefficient values of the synthesized

nanocomposite samples increased with increasing the density of the prepared samples. According to Equation 2, the HVL values decreased with increasing the density values of the fabricated sample [18], and as a result it shows that the efficiency of the shielding materials increased by decreasing HVL values. In addition, pursuant to Figure 4, with investigating the effect of thickness on the efficiency of the shield it can be realized that increasing the thickness and energy range of the samples has enhanced the HVL value of the samples and as a result decreased their shielding effectiveness [18,19].

The shielding efficiencies of nanocomposite samples were investigated by comparing the mass attenuation coefficient (μm) parameter in the radiology energy range. The obtained results for the samples are given in Table 4, illustrating that mass attenuation coefficient value of the samples decreased with increasing energy range. Furthermore, it demonstrates that the mass attenuation value of samples decreased as the thickness value of the nanocomposite samples increased. 2mm thickness of PE-A-25 showed the most effective shield compared to other samples and pure HDPE as shown in Figure 5. The results indicated that WO_3/Bi_2O_3/GO/HDPE nanocomposite samples had better shielding performance than $BaSO_4$/GO/HDPE samples due to their higher mass and linear attenuation coefficient, which originates from their higher atomic number [18, 20]

Morphological characterization of the synthesized nanocomposite samples

SEM microscopy was utilized to investigate morphology of the fabricated nanocomposite samples. SEM photos of the prepared nanocomposite samples (Figure 6) demonstrated good connectivity between the applied fillers and the polymer matrix used. According to the obtained images, there was complete wetting or impregnation between the nanoparticles and polymer. The aforementioned result is originated from the support and decoration of nanoparticles on the graphene oxide

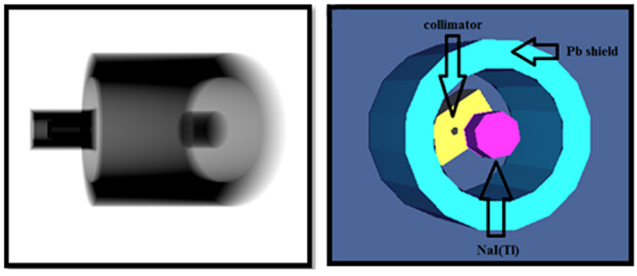

(a) (b)

Figure 3 A: Radiographic image of system components simulated by the VISED, B: 3D image of the components.

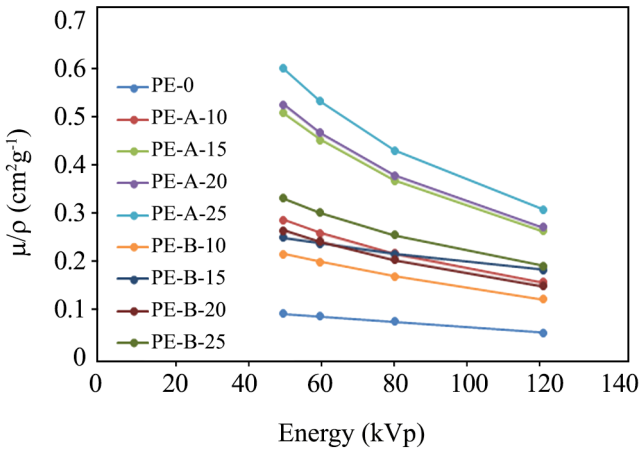

(a)

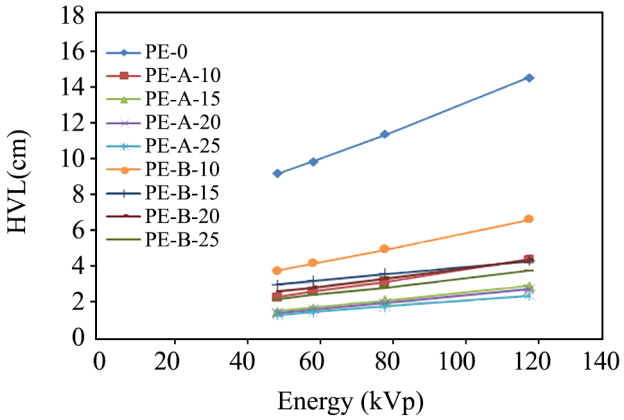

(b)

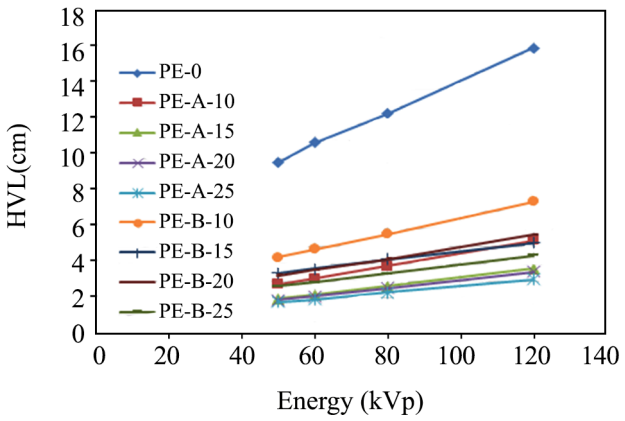

(c)

Figure 4. Half value layer (HVL) results of the synthesized nanocomposite samples (in thickness: (A) 2mm, (B) 4mm, and (C) 6 mm).

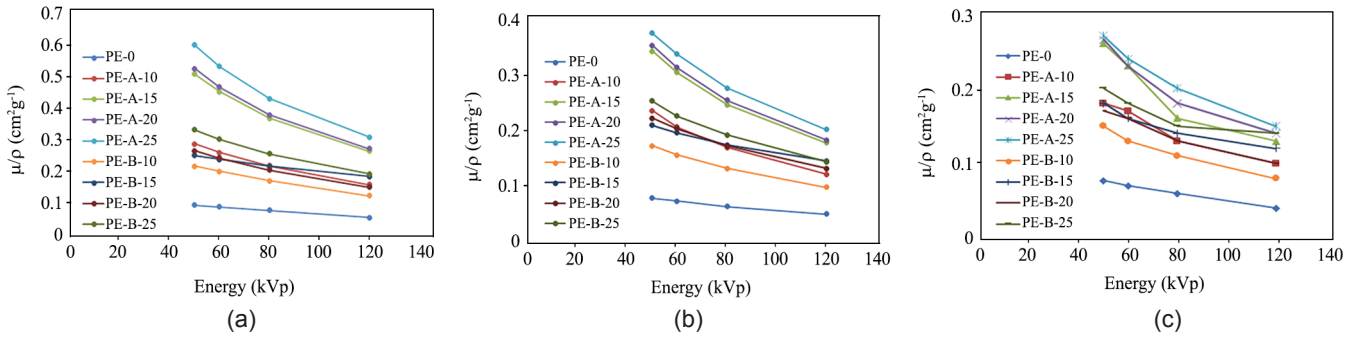

Figure 5. Measured mass attenuation coefficient results of the synthesized nanocomposite samples (in thickness: (A) 2mm, (B) 4mm, and (C) 6 mm).

surface, where the polyethylene chains are intertwined to the nanoparticles via graphene structure, and afterwards the mentioned mechanism leads to miscibility between the fillers used and the polymer media [21]. It can be claim that the presence of nanoparticles on the polymer bed is not obviously visible, which is a confirmation of the literature data [18,20]

Mechanical characterization of synthesized nanocomposite samples

To investigate the mechanical properties of samples, tensile and DMTA analysis were employed, which relates to the ratio of nanoparticles loaded in HDPE. The tensile test was used to measure mechanical properties. Figure 7 illustrates a comparison of the samples in the stress- strain curve. Table 5 demonstrates similar properties with their values. As shown in Table 5, increasing nanoparticles in HDPE matrix leads to a decrease in mechanical properties. On the other hand, Young's moduli of PE-B-25 and PE-A-25 have the highest value in comparison with other samples. As expected, the results demonstrate that barium sulfate/

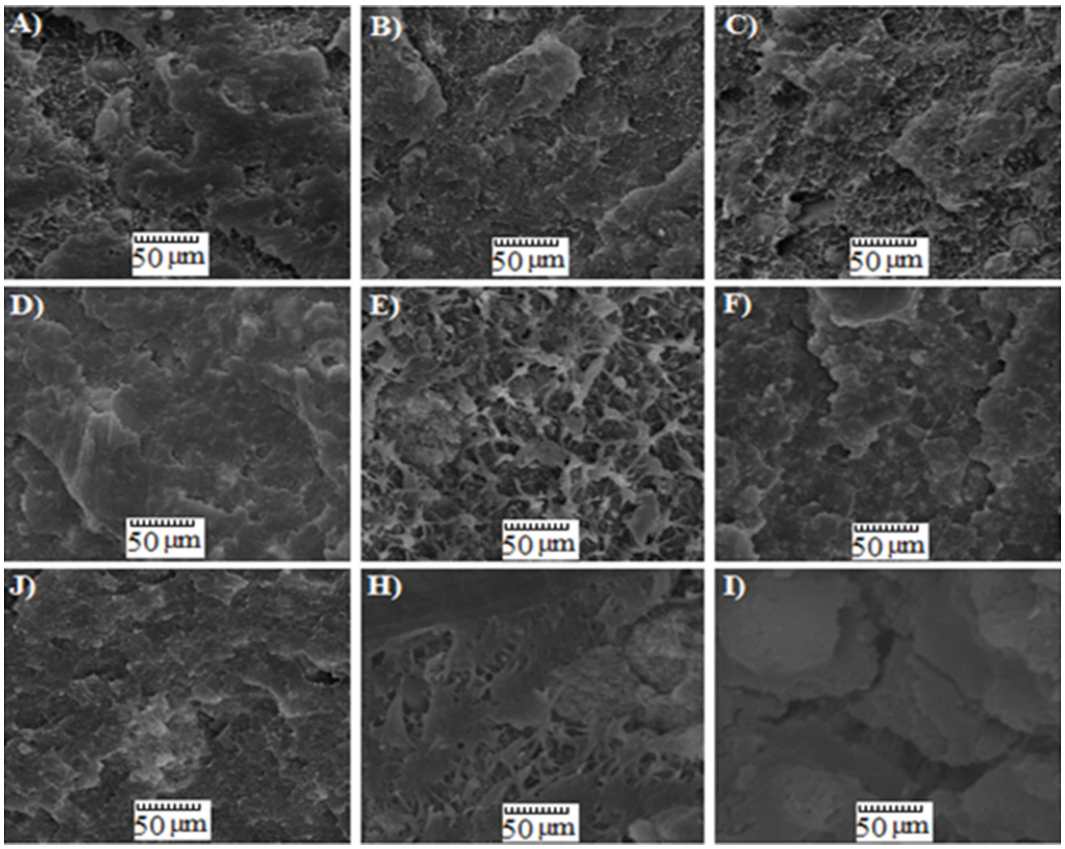

Figure 6. SEM images of A) PE-A-10, B) PE-A-15, C) PE-A-20, D) PE-A-25, E) PE-B-10, F) PE-B-15, J) PE-B-20, H) PE-B-25, and I) PE-0.

Table 5. Results of mechanical properties of nanocomposite samples.

Sample	σ_b (MPa)[a]	ε_b(%)[b]	E (MPa)[c]	T_g (°C)[d]	E′(GPa)[e]
PE-0	34.96± 1.5	122.3± 1.1	285.67± 0.1	-118± 0.3	2.3± 0.5
PE-A-10	17.38± 0.8	6.96± 1.4	249.43± 0.3	-111± 0.5	5.6± 0.2
PE-A-15	24.24± 2.3	9.34± 0.9	259.43± 0.2	-110± 0.2	6.6± 0.3
PE-A-20	24.00± 0.5	7.75± 2.0	278.78± 0.5	-110± 0.1	7.5± 0.1
PE-A-25	24.29± 2.2	8.08± 2.6	300.63± 1.3	-108± 0.5	8.1± 0.4
PE-B-10	21.39± 1.0	9.64± 1.9	221.91± 2.3	-113± 0.5	3.3± 0.7
PE-B-15	21.67± 2.6	7.93± 0.7	273.26± 3.0	-112± 0.4	3.6± 0.1
PE-B-20	20.16± 1.5	6.74± 1.4	299.02± 0.9	-110± 0.6	4.2± 0.3
PE-B-25	17.23±1.4	5.33± 1.1	323.14± 2.8	-108± 0.8	5.6± 0.5

[a]Tensile strength, [b]Elongation-at-break, [c]Young'smodulus, [d]Glass transition temperature obtained from tan delta curves, [e]E' is storage modulus at -120°C.

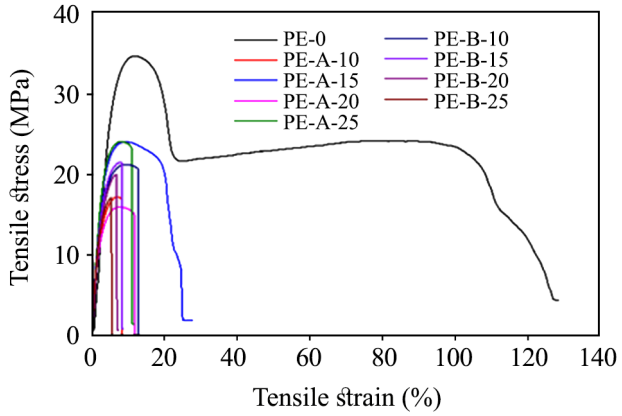

Figure 7. Stress-strain curves of nanocomposite samples.

HDPE nanocomposites compared to tungsten/bismuth/HDPE composites have higher Young's modulus values. However, in terms of tensile strength, HDPE/tungsten/bismuth composites performed better. Overall, it is observed that the tensile strength and Young's modulus of the samples increased with increasing nanoparticles, but decreased compared to HDPE [23].

To observe the effect of nano particle weight percentage on the glass transition temperature and storage modulus of nanocomposites, DMTA analysis was used. The curves obtained in Figure 8 and the results obtained are summarized in Table 5. According to Table 4, by increasing weight fraction of nanoparticles, storage modulus of nanocomposites increased and shifted to higher values. This result indicates the proper dispersion of nanoparticles in the polymer matrix. This phenomenon is due to the decoration of nanoparticles on the surface of GO [19]. Another aspect of this achievement showed that the increase in storage modulus values in the presence of tungsten/bismuth nanoparticles is greater than that of nanobarium sulfate. Figure 8 shows the tan δ curves of nanocomposite samples. The peaks in these curves show the glass transition temperature and due to them, with increasing the weight fraction of nanoparticles, the glass transition temperature of the samples has increased. This arises from preventing the movement of polymer chains by

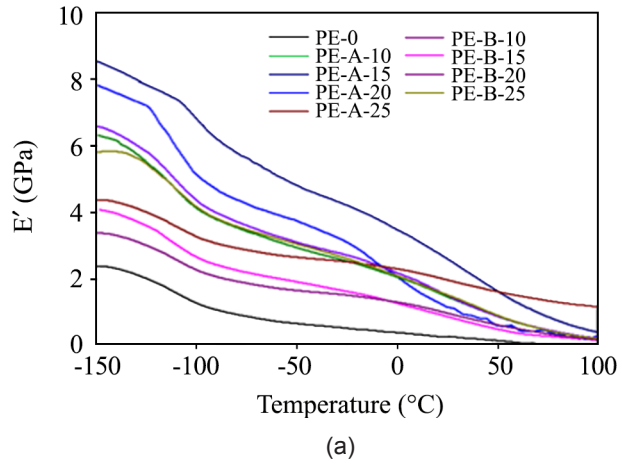

(a)

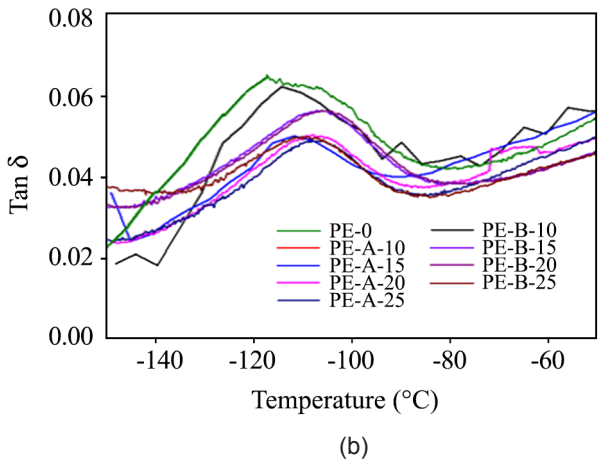

(b)

Figure 8. Storage modulus (E') and tan δ curves of nanocomposite samples.

increasing the weight fraction of nanoparticles [15, 26].

CONCLUSIONS

In this study, HDPE-based nanocomposites with different weight percentages of nano tungsten oxide, bismuth oxide, and barium sulfate were prepared and characterized via shielding and mechanical analysis. The performance of nanocomposites against X-ray radiations was investigated by calculating experimentally and simulating linear and mass attenuation coefficient, HVL and Hounsfield values. The results obtained demonstrated that by raising the weight fraction of the fillers used, the linear attenuation coefficient and also the absorbed dose values increased dramatically and HDPE with 25% concentration of WO_3/Bi_2O_3/GO showed superior shielding properties compared to other samples due to its relevant shielding parameters. X-ray radiation attenuation performance of HDPE with 25% concentration of WO_3/Bi_2O_3/GO composite in 50kvp was equal to 0.5 mm pure lead. The WO_3/Bi_2O_3/GO/HDPE composites showed more shielding performance compared to $BaSO_4$/GO/HDPE composites due to their higher atomic number. The mechanical properties of nanocomposites illustrated that, in the solid state, the 25 wt% WO_3/Bi_2O_3/GO-loaded composite still has a flexible behavior, despite the lower yield strain compared to neat HDPE.

ACKNOWLEDGEMENTS

Authors would like to acknowledge Behin Negar Co, Ltd, Tehran, Iran for providing advanced sample prep aration micro-CT imaging using their LOTUS-NDT scanner and image processing and analyses services and also Iran Polymer and Petrochemical Institute (IPPI) for financial support of this work.

CONFLICTS OF INTEREST

The authors declare that they have no conflicts of interest.

REFERENCES

1. Singh AK, Singh RK, Sharma B, Ajay Kumar Tyagi AK (2017) Characterization and biocompatibility studies of lead free x-ray shielding polymer composite for healthcare application. Radiat Phys Chem 138: 9-15
2. Lyra M, Charalambattou P (2011) Radiation protection of staff in 111In radionuclide therapy- is the lead apron shielding effective? Radiat Prot Dosim 147: 272-276
3. Aral N, Banu Nergis F, Candan C (2016) An alternative X-ray shielding material based on coated textiles. Text Res J 86: 803-811
4. Maghrabi HA, Vijayan A, Mohaddes F, Deb P, Wang L (2016) Evaluation of x-ray radiation shielding performance of barium sulphate-coated fabrics. Fiber Polym 17: 2047-2054
5. Guetersloh S, Zeitlin C, Heilbronn L, Miller J, Komiyama T, Fukumura A (2006) Polyethylene as a radiation shielding standard in simulated cosmic-ray environments. Nucl Instrum Meth B 252: 319-332
6. Shavers MR, Zapp N, Barber RE, Wilson JW, Qualls G, Toupes L (2004) Implementation of ALARA radiation protection on the ISS through polyethylene shielding augmentation of the Service Module Crew Quarters. Adv Space Res 34: 1333-1337
7. Adams J, Hathaway D, Grugel R, Watts J, Parnell T, Gregory J, Winglee RM (2005) Revolutionary concepts of radiation shielding for human exploration of space. Nasa Technical Reports: 1-110
8. Nambiar S, Yeow JTW (2012) Polymer-composite materials for radiation protection. ACS Appl Mater Interfaces 4: 5717-5726
9. Mahmoud ME, El-Khatib AM, Badawi MS, Rashed AR, El-Sharkawy RM, Thabet AA (2017) Fabrication, characterization and gamma rays shielding properties of nano and micro lead oxide-dispersed-high density polyethylene composites. Radiat Phys Chem 145: 160-173
10. Belgin EE, Aycik GA (2015) Preparation and radiation attenuation performances of metal oxide filled polyethylene based composites for ionizing electromagnetic radiation shielding

applications. J Radioanal Nucl Ch 306: 107-117
11. Kaloshkin SD, Tcherdyntsev VV, Gorshenkov MV, Gulbin VN, Kuznetsov SA (2012) Radiation-protective polymer-matrix nanostructured composites, J Alloys Compound. 536: S522- S526
12. Laurenzi S, de Zanet G, Santonicola MG (2020) Numerical investigation of radiation shielding properties of polyethylenebased nanocomposite materials in different space environments. Acta Astronaut 170: 530-538
13. Afshar M, Morshedian J, Ahmadi S (2019) Radiation attenuation capability and fow characteristics of HDPE composite loaded with W, MoS2, and B4C. Polym Compos 40:149-158
14. Ji Chen, Bowen Yao, Chun Li, Gaoquan Shi (2013) An improved Hummers method for eco-friendly synthesis of graphene oxide. Carbon 64: 225-229
15. Hummers Jr WS, Offeman RE (1958) Preparation of graphitic oxide. J Am Chem 80: 1339-1339
16. Hashemi SA, Mousavi SM, Faghihi R, Arjmand M, Sina S, Amani AM (2018) Lead oxide-decorated graphene oxide/epoxy composite towards X-Ray radiation shielding. Radiat Phys Chem 146: 77-85
17. Mheemeed AK, Hasan HI, Al-Jomaily FM (2017) Gamma-ray absorption using rubber-lead mixtures as radiation protection shields. J Radiat Nuclear Chem 29: 653-659
18. Tohid Abdolahzadeh T, Morshedian J, Ahmadi S, Ay MR, Mohammadi O (2021) Introducing a novel Polyvinylchloride/Tungsten composites for shielding against gamma and X- ray radiations. Iran J Nucl Med 29: 58-64
19. Bagheri K, Razavi SM (2018) Thermal resistance, tensile properties, and Gamma radiation shielding performance of unsaturated polyester/nanoclay/PbO composites. Radiat Phys Chem 146: 5-10
20. Mahmoud ME, El-Khatib AM, Badawi MS, Rashed AR, El-Sharkawy RM, Thabet AA (2018) Recycled high-density polyethylene plastics added with lead oxide nanoparticles as sustainable radiation shielding materials. J Clean Produc 176: 276-287
21. Mota EG, Rockenbach MIB, da Costa NP, Rigo A, Coelho CRR (2008) Radiopacity of impression materials using an indirect digital system. Rev Odonto Ciência 23: 333-337
22. Obaid SS, Gaikwad DK, Pawar PP (2018) Determination of gamma ray shielding parameters of rocks and concrete. Radiat Phys Chem 144: 356-360
23. Akkurt I, Akyıldırım H, Mavi B, Kilincarslan S, Basyigit C (2010) Photon attenuation coefficients of concrete includes barite in different rate. Ann Nucl Energy 37: 910-914
24. Chen S, Bourham M, Rabiei A (2015) Attenuation efficiency of X-ray and comparison to gamma ray and neutrons in composite metal foams. Radiat Phys Chem 117: 12-22
25. Hanifpour A, Bahri-Laleh N, Nekoomanesh-Haghighi M, Karimi M; Synthesis and characterization of poly1-hexene/silica nanocomposites. Polym Test 61: 27-34
26. Hanifpour A, Bahri-Laleh N, Nekoomanesh-Haghighi M (2020) Methacrylate functionalized POSS as an efficient adhesion promoter in olefin-based adhesives. Polym Eng Sci 60: 2991-3000